Fast computation of time-dependent acoustic fields

Michael Carley[a)]
Department of Mechanical Engineering, University of Bath, Bath BA2 7AY, United Kingdom

Ghader Ghorbaniasl
Vrije Universiteit Brussel (VUB), Pleinlaan 2, 1050 Brussels, Belgium

(Received 23 August 2016; revised 28 October 2016; accepted 7 November 2016; published online 23 November 2016)

A method for the fast evaluation of time-dependent acoustic fields from complex sources is presented. The technique is based on a fast integration method for the boundary integral arising in a Kirchhoff formulation and requires a small, and roughly constant, computation time to compute a transient signal, at the expense of a pre-processing stage. In the calculations in this paper, based on test cases for a single rotor, a counter-rotating open rotor, and a broadband volume source, it is found that transient field calculations require an order of magnitude less computational time for the field from an array of 16 384 sources, a computational advantage that increases with source number.
 [http://dx.doi.org/10.1121/1.4968018]

[NAG] Pages: 3963–3970

I. INTRODUCTION

The "solution" of many acoustic problems is the field radiated by a source. Given the source, the field can always be computed, but may require more computation time than is practical so that simple knowledge of the source is not sufficient for useful determination of the field. There are methods that replace a source with a simpler equivalent source that can be used to compute the field more quickly, thus making the computation feasible in some reasonable time. For single frequency fields, a multipole expansion is the classical approach and can be derived for the field generated by sources of arbitrary shape,[1] based on the work of Oestreicher.[2] Similar methods exist in more specialized contexts, such as a recently developed technique for the far-field noise of a propeller, using data from a small number of near-field points to generate an equivalent expansion,[3] or the approach developed for quadrupole terms arising from flow noise.[4]

When a transient signal is required, however, methods for equivalent expansions or replacement sources are less common. There is a requirement for such methods, in particular, in aeroacoustics, where signals are often broadband and sources, for example, those generated by computational fluid dynamics (CFD) calculations, may have millions of points, for example, in jet noise problems. The signal must typically be computed over a large domain, orders of magnitude larger than the source region, and at a sub-wavelength scale in order to avoid spatial aliasing and to properly resolve phenomena in the radiated field. For example, in a study of an accelerated computation method,[5,6] the authors estimated that standard evaluation would require 6.5 days CPU time to compute a 755 time point signal at 2.3×10^4 field points using a source with 1.6×10^6 source points generated by a mixing layer calculation. Clearly, in any realistic problem, acceleration methods are required in order to make detailed transient field calculations feasible.

Recently, one of us[7] has developed a method based on time-domain spherical harmonics which uses a relatively small number of near-field evaluations to generate a multipole expansion which can be used to compute the radiated field outside some surface enclosing the source. The method is quite general and requires only pressure evaluations on a set of spherical surfaces around the source. In this paper, we present a method which requires as input the field on only one surface, but at the expense of requiring the time derivative and gradient of pressure as well as the pressure proper. The technique is based on a Kirchhoff method for the radiation problem and can also be used on other boundary-integral formulations. The required input is some means of computing the pressure, pressure derivative, and pressure gradient at required points on a spherical surface, and the output is the transient signal at points on some radial vector from the center of the sphere.

II. ANALYSIS

The method which we present is based on a boundary integral formulation for the radiated field outside some surface on which any necessary quantities can be evaluated. We employ a Kirchhoff formulation, but the approach is identical for any other boundary integral equation for the field.[8] The Kirchhoff integral for acoustic pressure p outside a closed surface S is[1]

$$4\pi p(\mathbf{x},t) = \int_S \left[\hat{\mathbf{r}}\cdot\hat{\mathbf{n}}_1 \left(\frac{\dot{p}_1(\mathbf{x}_1,\tau)}{Rc} + \frac{p_1(\mathbf{x}_1,\tau)}{R^2} \right) - \frac{1}{R}\frac{\partial p_1}{\partial n_1} \right] \mathrm{d}S(\mathbf{x}_1),$$
$$\mathbf{r} = \mathbf{x} - \mathbf{x}_1,\ R = |\mathbf{r}|,\ \hat{\mathbf{r}} = \mathbf{r}/R,\ \tau = t - R/c, \qquad (1)$$

where $\hat{\mathbf{n}}_1$ is the outward pointing unit normal on the surface, $\partial p_1/\partial n_1 = \hat{\mathbf{n}}_1.\nabla p_1$, and subscript 1 denotes a variable of integration. Observer and source positions are $\mathbf{x}$ and $\mathbf{x}_1$,

a)Electronic mail: m.j.carley@bath.ac.uk

respectively, with corresponding reception and retarded times t and τ. Speed of sound is c and a dot denotes time differentiation.

In spherical polar coordinates (ρ, θ, ϕ) with S a spherical surface of radius a centered on the origin, Eq. (1) becomes

$$\begin{aligned} 4\pi p(\mathbf{x},t) = a^2 \int_0^{\pi}\int_0^{2\pi} \left[\hat{\mathbf{r}}.\hat{\mathbf{n}}_1 \left(\frac{\dot{p}_1(\mathbf{x}_1,\tau)}{Rc} + \frac{p_1(\mathbf{x}_1,\tau)}{R^2}\right) - \frac{1}{R}\frac{\partial p_1}{\partial n_1}\right] \\ \times \mathrm{d}\phi_1 \sin\theta_1 \mathrm{d}\theta_1, \\ \hat{\mathbf{n}}_1 = (\sin\theta_1\cos\phi_1, \sin\theta_1\sin\phi_1, \cos\theta_1), \mathbf{x}_1 = a\hat{\mathbf{n}}_1, \\ \mathbf{x} = \rho(\sin\theta\cos\phi, \sin\theta\sin\phi, \cos\theta). \end{aligned} \tag{2}$$

Given the required quantities on the sphere, the radiated field can be computed at any point via the surface integral. In this form, however, the computational effort is constant and large for evaluation of the field at any point $\mathbf{x}$. We propose a technique which, at the expense of some pre-processing, accelerates the calculation on rays of constant (θ, ϕ), by exploiting a coordinate transformation and some standard interpolation techniques. Subsequent sections detail these techniques and how they are combined to yield an accelerated field computation method.

A. Spectral interpolation on the sphere

Our approach is based on source distributions on the spherical surface at discrete time steps. We have some freedom in our choice of interpolation method, so we choose a spectral method based on an expansion in spherical harmonics,[9]

$$\begin{aligned} f(\theta,\phi) = \sum_{n=0}^{\infty}\sum_{m=0}^{n} \bar{P}_n^m(\cos\theta)[a_{n,m}\cos(m\phi) \\ + b_{n,m}\sin(m\phi)], \end{aligned} \tag{3}$$

where $\bar{P}_n^m(\theta)$ is the normalized associated Legendre function,

$$\bar{P}_n^m(\theta) = \left[\frac{2n+1}{2}\frac{(n-m)!}{(n+m)!}\right]^{1/2} P_n^m(\cos\theta). \tag{4}$$

Discretizing the surface into a suitable set of nodes for cubature in θ and ϕ, using Gauss-Legendre and trapezoidal rules, respectively, the coefficients in the expansion of Eq. (3) are given by

$$a_{n,m} = \frac{2}{N_\phi}\sum_{i=0}^{N_\theta-1}\sum_{j=0}^{N_\phi-1} \bar{P}_n^m(\cos\theta_i)\cos(m\phi_j) w_i^\theta f(\theta_i,\phi_j), \tag{5a}$$

$$\begin{aligned} b_{n,m} = \frac{2}{N_\phi}\sum_{i=0}^{N_\theta-1}\sum_{j=0}^{N_\phi-1} \bar{P}_n^m(\cos\theta_i)\sin(m\phi_j) w_i^\theta f(\theta_i,\phi_j), \\ \text{where } \phi_j = \frac{2\pi j}{N_\phi}, \end{aligned} \tag{5b}$$

where the azimuthal integration is carried out using an N_ϕ point trapezoidal rule and $\cos\theta_i$ and w_i^θ are the nodes and weights of an N_θ-point Gauss−Legendre quadrature rule. Coefficients with $m = 0$ must be multiplied by 1/2.

This integration is implemented as a matrix multiplication of the vector $\mathbf{f}$ of source terms at the nodes. If $\mathbf{a}$ is the vector of coefficients $a_{n,m}$, $b_{n,m}$, then

$$\mathbf{a} = \mathbf{A}\mathbf{f}, \tag{6}$$

and the entries of the $\mathbf{A}$ are given by Eq. (5).

To evaluate the function at some point on the sphere, we construct a vector of spherical harmonics,

$$\mathbf{p}(\theta,\phi) = [\cdots \cos(m\phi)\bar{P}_n^m(\cos\theta) \quad \sin(m\phi)\bar{P}_n^m(\cos\theta) \cdots], \tag{7}$$

and the interpolated value at (θ, ϕ) is given by

$$f(\theta,\phi) \approx [\mathbf{p}(\theta,\phi)\mathbf{A}]\mathbf{f}, \tag{8}$$

where the term in parentheses can be implemented as a single vector of length $N_p = N_\theta N_\phi$ and the interpolation reduces to an inner product with the function values $\mathbf{f}$. Only one $N_p \times N_p$ matrix $\mathbf{A}$ is required and is common to all spheres discretized with the same N_θ and N_ϕ, independent of radius a, so it can be pre-computed and re-used as necessary.

B. Integration on the sphere

To evaluate the acoustic integrals over the spherical surface, we take advantage of the separable coordinate system and evaluate quantities in stages so that as much as possible of the work is reusable. We begin by adopting a new coordinate system on the spherical surface, (ψ, γ), Fig. 1. This rotates the original system to be oriented about the radial vector from the sphere center to the field point and yields an integration method which gives the transient signal at all points on that radius vector for very little additional effort. From Fig. 1, it is clear that points at a given value of ψ on the surface are circles at constant distance R from points on the radial vector. This is equivalent to grouping points on the sphere with the same retarded time relative to the field point.

Equation (2) can be rewritten in the new coordinate system, yielding

$$\begin{aligned} 4\pi p(\mathbf{x},t) = a^2 \int_0^{\pi}\left[\frac{\hat{\mathbf{r}}.\hat{\mathbf{n}}_1}{Rc}\int_0^{2\pi}\dot{p}_1(\psi,\gamma,\tau)\,\mathrm{d}\gamma \right. \\ + \frac{\hat{\mathbf{r}}.\hat{\mathbf{n}}_1}{R^2}\int_0^{2\pi} p_1(\psi,\gamma,\tau)\,\mathrm{d}\gamma \\ \left. - \frac{1}{R}\int_0^{2\pi}\frac{\partial p_1}{\partial n_1}\,\mathrm{d}\gamma\right]\sin\psi\,\mathrm{d}\psi, \\ R(\psi) = \left(\rho^2 - 2a\rho\cos\psi + a^2\right)^{1/2}, \end{aligned} \tag{9}$$

noting that R, $\hat{\mathbf{r}}$, and τ are functions of ψ only.

The integration over the sphere is implemented as a matrix multiplication on the surface, which requires interpolation onto the rotated surface coordinate system. This rotation could be performed using efficient procedures for the spherical harmonic expansion[10] and would require $O(N_\theta^3)$ operations. Since we do not require the spherical harmonic

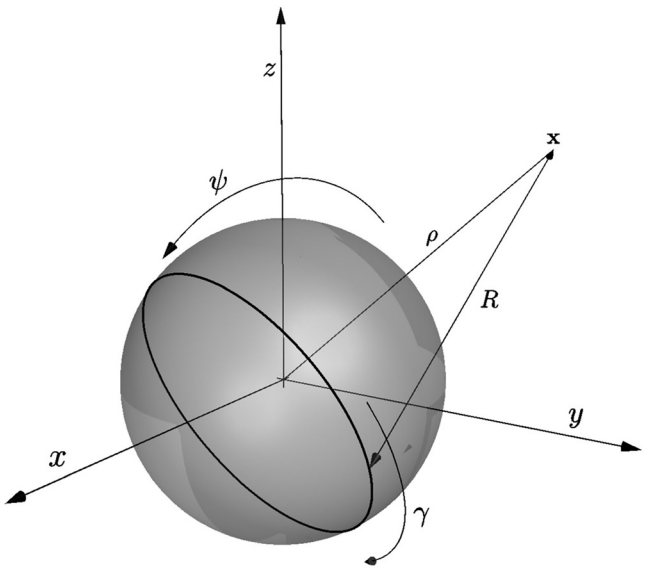

FIG. 1. Auxiliary coordinate system for surface integration.

coefficients or the interpolation surface quantity explicitly, but only integrals of surface data, we find it more convenient to pre-compute quadrature matrices which give integrals in $O(N_\theta^2)$ operations per quadrature node in ψ.

Conversion between the original and transformed coordinate system is accomplished using

$$\phi_1 = \tan^{-1}\frac{\sin\theta\sin\phi\cos\psi - A\cos(\gamma+\alpha)\sin\psi}{\sin\theta\cos\phi\cos\psi + B\sin(\gamma+\beta)\sin\psi}, \tag{10a}$$

$$\theta_1 = \cos^{-1}[\cos(\theta+\psi) + \sin\theta\sin\psi(1-\sin\gamma)], \tag{10b}$$

$$A^2 = 1-\sin^2\phi\sin^2\theta, \quad \alpha = \tan^{-1}(\tan\phi\cos\theta);$$
$$B^2 = 1-\cos^2\phi\sin^2\theta, \quad \beta = \tan^{-1}(\tan\phi/\cos\theta).$$

The integration in γ is performed using a trapezoidal rule which yields spectral accuracy for periodic functions,

$$\int_0^{2\pi} f(\gamma)\,\mathrm{d}\gamma \approx \frac{2\pi}{N_\gamma}\sum_0^{N_\gamma-1} f(\gamma_i), \qquad \gamma_i = 2\pi i/N_\gamma, \tag{11}$$

which, with the use of the interpolation matrix of Sec. II A, gives

$$\int_0^{2\pi} f(\gamma)\,\mathrm{d}\gamma \approx \frac{2\pi}{N_\gamma}\sum_0^{N_\gamma-1}\left\{\mathbf{A}^T\mathbf{p}\left[\theta(\gamma_i),\phi(\gamma_i)\right]\right\}^T\mathbf{f} = \mathbf{q}(\psi)\mathbf{f},$$
$$\mathbf{q}(\psi) = \frac{2\pi}{N_\gamma}\left\{\mathbf{A}^T\sum_0^{N_\gamma-1}\mathbf{p}\left[\theta(\gamma_i),\phi(\gamma_i)\right]\right\}^T. \tag{12}$$

The vector $\mathbf{q}(\psi)$ of length N_p gives the integral over γ at ψ via the inner product $\mathbf{q}\cdot\mathbf{f}$. The size of $\mathbf{q}$ is independent of N_γ and its entries for a given direction (θ,ϕ) depend only on ψ and the discretization of the sphere, N_θ and N_ϕ, so that it can be computed once for all problems independent of source type and sphere radius, with no penalty for using a large value of N_γ.

Integration in ψ is performed using a Gaussian quadrature of length N_ψ with nodes ψ_i and weights w_i^ψ, $i=0,\ldots,N_\psi-1$. Defining the surface source distribution $\boldsymbol{\sigma}(\tau)$,

$$\boldsymbol{\sigma}(\tau) = \begin{bmatrix} \dot p_0(\tau) & \partial p_0(\tau)/\partial n & p_0(\tau) \\ \dot p_1(\tau) & \partial p_1(\tau)/\partial n & p_1(\tau) \\ & \vdots & \\ \dot pN_{p-1}(\tau) & \partial pN_{p-1}(\tau)/\partial n & pN_{p-1}(\tau) \end{bmatrix}, \tag{13}$$

the integrals over γ at a node ψ_i are given by

$$\frac{a^2}{4\pi}\mathbf{q}(\psi_i)\boldsymbol{\sigma}(\tau) \approx \frac{a^2}{4\pi}\left[w_i\sin\psi_i\int_0^{2\pi}\dot p\,\mathrm{d}\gamma \times w_i\sin\psi_i\int_0^{2\pi}\partial p/\partial n\,\mathrm{d}\gamma\; w_i\sin\psi_i\int_0^{2\pi} p\,\mathrm{d}\gamma\right], \tag{14}$$

noting that τ is a function of ψ.

The integrals at each quadrature node are evaluated using a single matrix multiplication using $\mathbf{Q}\boldsymbol{\sigma}(\tau)$,

$$\mathbf{Q} = \frac{a^2}{4\pi}\begin{bmatrix} w_0\sin\psi_0\mathbf{q}(\psi_0) \\ w_1\sin\psi_1\mathbf{q}(\psi_1) \\ \vdots \\ w_{N_\gamma-1}\sin\psi_{N_\gamma-1}\mathbf{q}\left(\psi_{N_\gamma-1}\right) \end{bmatrix}. \tag{15}$$

As described in Sec. II C, for computational efficiency this is evaluated for the source terms at a single value of τ and an advanced-time algorithm is used to interpolate the pressure contributions at corresponding reception times t. The matrix $\mathbf{Q}$ is of size $N_p\times N_\psi$ so that if $N_\psi = O(N_\theta)$ to avoid aliasing, the computational effort is $O(N_\theta^3)$.

We note that by decoupling directivity and distance in the calculation, the matrix multiplication of Eq. (15) is required only once per time point on each radial vector, with a small additional effort to compute the field at a particular point on that vector. Geometrically, this approach can be seen as replacing the spherical Kirchhoff surface with a direction-dependent linear distribution of point sources.

C. Advanced time interpolation

The procedure of Sec. II B gives the inner integral over γ at points in ψ on the spherical surface, the first stage in evaluating the retarded potential for $p(\rho,\theta,\phi,t)$. These inner integrals do not, however, contribute to the radiated pressure simultaneously and their contributions must be summed appropriately into the transient signal. This is performed using an advanced-time, or source-time-dominant technique,[11,12] in which the reception time $t=\tau+R/c$ is computed and the contribution to the radiated pressure is interpolated into the signal.

For a pressure calculation with $p(t)$ a function $g(\tau)$ of τ,

$$p(t) = g(\tau), \tag{16}$$

for example, $g(\tau) = q(\tau)/4\pi R$, the algorithm works as follows. Reception time t and retarded time τ are discretized with the same time step Δt. We write $t_i = i\Delta t$, $q_i = q(\tau_i)$, and $p_i = p(t_i)$. Starting from retarded time τ, we write

$$t = \tau + R/c,$$

and for interpolation,

$$t = (i + \delta)\Delta t,$$

where i is an integer and $0 \le \delta < 1$. Given some interpolation method for equally spaced data, we write

$$f(\delta) = \sum_{k=k_0}^{k_1} w_k f(k), \tag{17}$$

where the weights w_k are generated by the interpolation scheme (we use Lagrange) and k_0 may be less than zero. To increment p, we take $\Delta p = g(\tau)$ and for each k, $k_0 \le k \le k_1$,

$$p_{i+k} := p_{i+k} + w_k \Delta p.$$

This is equivalent to a sparse matrix multiplication, though it is implemented in our code as a sequence of summations.

The algorithm is identical for any source term as long as Δp can be computed, and since the weights are functions of R and Δt only, they can be pre-computed and stored. To compute the radiated field, the source terms at each retarded time τ_i are used to evaluate the contribution to the field at corresponding advanced times t_{i+k}, with contributions being summed in-place to give an overall final signal for the whole retarded time period. This has the particular advantage that each set of source terms need be read only once, rather than storing them in memory and interpolating on retarded time, a considerable saving in effort on large data sets.

D. Computational demands

The computational effort for field calculation is readily estimated from Secs. II A and II B. We neglect setup costs for matrices, since these can be generated once and are universally applicable once the spherical grid has been chosen. The computational effort per time point for a field point on one radius vector is

$$T = a_1 N_p N_\psi + a_2 N_\psi N_i, \tag{18}$$

where N_i is the number of points in the interpolation of Eq. (17), e.g., four for third-order interpolation, and a_1 and a_2 are implementation-dependent constants. In any reasonable calculation, $N_p N_\psi \gg N_\psi N_i$, and the computational cost per radial vector scales as $N_p N_\psi$, with the marginal cost per point $N_\psi N_i$ very small, as will be shown in the performance evaluation of the method, The computational time is independent of source complexity once the spherical grid has been set, so that the method is increasingly efficient for more complex sources, but is not competitive for simple problems, as will become clear when performance data are presented later.

If a whole-field calculation is to be performed, with the same resolution as the spherical grid, the calculation must be performed for N_p radial vectors, with the same procedure being applied for each radius independently, and spherical harmonic interpolation being used to find the field at any required point. The total number of evaluations required for the radial vector data could be reduced by exploiting symmetries, but the effort will still scale as N_p.

If source data on the sphere are being interpolated from a CFD calculation, say, there is effectively no computational cost in generating them. If, as in our test cases, the field is computed from an array of point sources, there is a pre-processing cost in generating the surface data of $O(N_p N_s t_s)$, where t_s is the computational time for one source point and N_s is the number of point sources. When $N_p \ll N_s$, the computational effort for field evaluation is still very much faster than direct evaluation of the field. The break-even point where our approach is faster than direct evaluation of the field thus depends on the number of field points, their geometry, and the source data.

E. Summary of algorithm

The steps in the algorithm can be summarized as follows, given some means of computing p, $\dot{p}$ and $\partial p/\partial n$ on a surface.

1. Initialization

(a) Fix the sphere discretization N_θ and N_ϕ and compute matrix **A** from Eq. (5);
(b) fix quadrature rule length N_ψ and generate **Q** for the required radial vector (θ, ϕ), using Eq. (15).

2. Pre-processing

(a) Fix the sphere radius a to enclose all sources;
(b) for each point (θ, ϕ) on the sphere surface compute p, $\dot{p}$, and $\partial p/\partial n$ to generate $\boldsymbol{\sigma}$ at each time step, Eq. (13).

3. Computation

(a) For each ρ on radial vector (θ, ϕ), compute time interpolation weights from Eq. (17);
(b) for each time point, compute $\mathbf{Q}\boldsymbol{\sigma}$ and accumulate weighted sum, Eq. (17).

The output is a set of computed transient signals at the required points (ρ, θ, ϕ). Note that the matrices **A** and **Q** are problem-independent and need be evaluated once only for all calculations.

III. NUMERICAL TESTING

We present three sets of calculations designed to assess the performance of the method in terms of accuracy and computation time. The first case, which models a rotating

point source, represents the most basic problem which we might wish to solve, and gives a means of assessing accuracy and computation time. The second test case is a model problem for a counter-rotating open rotor (CROR) where transient non-periodic effects must be captured if the radiated field is to be properly modeled. This is the type of problem for which our technique is intended and thus a relevant, and demanding, test case. The final test uses a broadband volume source and is a check of the ability of our method to deal with problems characteristic of flow-generated noise.

In each case, we compute a transient signal at 65 points on a ray (ρ, θ, ϕ), $2 \le \rho \le 10$, $\theta = \pi/2$, $\phi = 1/2$. The enclosing sphere has radius $a = 1$. To assess error, we employ the measure

$$\epsilon = \frac{\max|p_d(\mathbf{x}, \mathbf{t} - p_f(\mathbf{x}, t)|}{\max|p_d(\mathbf{x}, t)|}, \tag{19}$$

where p_d and p_f are the time signals computed using the direct and fast methods, respectively. Error is reported for $\rho = 2$, but is roughly constant over the whole range in the calculations. Parameters varied are surface resolution N_θ, quadrature order N_ψ, time step Δt, and interpolation order for the advanced-time method. The azimuthal surface resolution N_ϕ is fixed at $N_\phi = 2N_\theta$. In some cases, where additional information about the source is known, computations could be accelerated by reducing N_ϕ, for example, when the field is known to be axisymmetric, but we concentrate here on the general case.

A. Rotating source

Sound generation by a rotating system is modeled by a ring source, with acoustic field given by

$$p(\mathbf{x}, t) = \int_0^{2\pi} \frac{\cos(n\Omega\tau - n\phi_1)}{4\pi R}\, \mathrm{d}\phi_1,$$
$$\mathbf{x}_1 = (r\cos\phi, r\sin\phi, 0), \quad \mathbf{r} = \mathbf{x} - \mathbf{x}_1, \quad R = |\mathbf{r}|. \tag{20}$$

This corresponds to the nth azimuthal order component of the field generated by a point source at radius r rotating at angular velocity Ω. The field is evaluated using a trapezoidal rule of length N_s in ϕ equivalent to discretizing the system into N_s point sources.

In order to avoid spatial aliasing, the spherical grid must be dense enough to capture the azimuthal variation of the field, i.e., $N_\phi > 2n$. We set rotor parameters $n = 7$, $r = 0.7$ m, and $\Omega = 400$ rad/s corresponding to a rotation Mach number $\Omega r/c = 0.82$ for a speed of sound $c = 340$ m/s. This rotation Mach number is at the upper end of the range to be expected in aeronautical applications.

Figure 2 shows the error behavior as a function of time step and interpolation order. The upper plot shows the solution converging to an error of about 10^{-5} on a properly resolved surface mesh, $N_\phi = 64$. The quadrature order N_ψ is also sufficiently large to avoid spatial aliasing, and so the error behavior is controlled by the time step. The lower plot shows the effect of varying the order of time interpolation

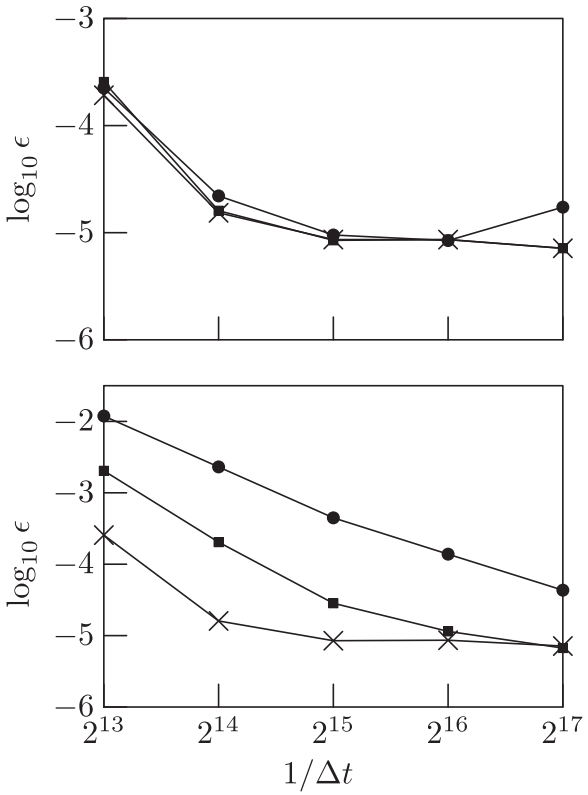

FIG. 2. Error versus time step for $N_\theta = 32$, $N_s = 8192$: upper plot, third-order time interpolation, circles $N_\psi = 16$; squares $N_\psi = 32$; crosses $N_\psi = 64$; lower plot, $N_\psi = 32$, circles, first order interpolation; squares, second order; crosses, third order.

and as might be expected, the linear interpolation shows the largest error and slowest convergence while second order is better and reaches the same accuracy as third order at the smallest time step considered.

In Fig. 3, we consider the effect of surface discretization at fixed time step and the effects of aliasing and/or inadequate surface resolution become apparent: at $N_\theta = 8$, the error is large but immediately drops at $N_\theta = 16$, a value large enough to properly resolve the surface pressure field. Increasing N_θ beyond this point does little to improve the accuracy since the spatial frequency content has been captured exactly.

B. Counter-rotating open rotor

Our second test case is one which is relevant to computationally demanding applications where a transient signal must be accurately captured. It is a model problem for a CROR, a system which generates quite complex waveforms owing to the interaction between two rotors of unequal blade number and/or rotation speed. We model the field as

$$p(\mathbf{x}, t) = \int_0^a \int_0^{2\pi} \frac{\cos(n_1\Omega_1\tau_1 - n_1\phi_1)}{4\pi R_1}\, \mathrm{d}\phi_1 r_1\, \mathrm{d}r_1$$
$$+ \int_0^a \int_0^{2\pi} \frac{\cos(n_2\Omega_2\tau_2 - n_2\phi_2)}{4\pi R_2}\, \mathrm{d}\phi_2 r_2\, \mathrm{d}r_2,$$
$$R_i = |\mathbf{x} - \mathbf{x}_i|, \quad \mathbf{x}_i = (r\cos\phi, r\sin\phi, z_i), \quad \tau_i = t - R_i/c, \tag{21}$$

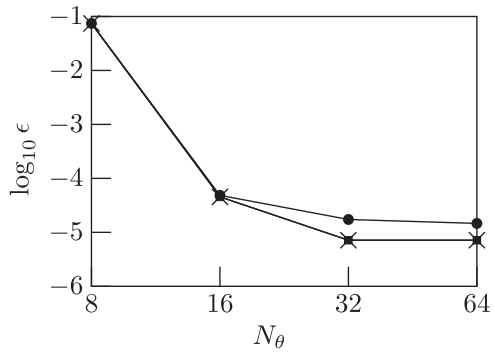

FIG. 3. Error versus N_θ, $\Delta t = 1/2^{17}$; circles: $N_\psi = 16$; squares: $N_\psi = 32$; crosses: $N_\psi = 64$.

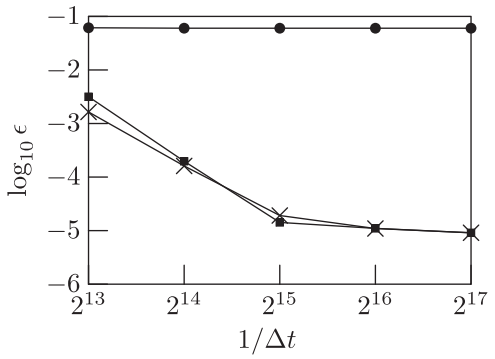

FIG. 5. Error versus time step for CROR test case with $N_\theta = 64$, $N_s = 16384$, third-order time interpolation: circles $N_\psi = 16$; squares $N_\psi = 32$; crosses $N_\psi = 64$.

where $z_{1,2}$ is the axial position of a rotor, the rotational frequencies $\Omega_{1,2}$ are unequal and of opposite sign and the harmonic numbers $n_{1,2}$ are not necessarily equal. For the tests presented here, we use the parameters of a published test case[13] with two eight-bladed rotors each of radius 0.381 m rotating at −4800 and 5200 rpm, respectively. We examine the signal generated by the interaction of two different harmonics of rotation frequency and set $n_1 = 8$ and $n_2 = 16$. As in the ring source case, the field is evaluated using a trapezoidal rule in azimuth and radius, equivalent to replacing the surface with a dense array of point sources, allowing an assessment of the computational burden as a function of source resolution.

Figure 4 shows a computed sample signal for one rotation period, $2\pi/|\Omega_1|$, of the front blade row. The transient effects caused by the interaction of the two blade row signals are apparent, with an underlying signal of frequency $8|\Omega_1|$ modulated non-periodically by its interaction with the signal of frequency $16|\Omega_2|$. Such transient effects must be correctly computed if the noise from CRORs is to be properly assessed in aeronautical applications.

Figure 5 shows the error behavior for the $N_\theta = 64$ grid as a function of time step and N_ψ. As is clear from the first curve on the plot, there is aliasing when N_ψ is too small (there is a similar problem when N_θ or N_ϕ are too small) and cannot adequately resolve the field on the spherical surface. This is to be expected: the minimum adequate sampling for the spherical surface is twice the maximum azimuthal order, in this case $N_\phi > 2|n_2| = 32$, corresponding to $N_\theta > 16$. For a surface grid of given resolution, any resampling must also respect the Nyquist criterion, so $N_\psi > 16$ to avoid aliasing. As soon as N_ψ is large enough, the error drops and is controlled by the temporal interpolation, rapidly reaching its minimum of 10^{-5}. Behavior for the $N_\theta = 32$ grid is quantitatively similar.

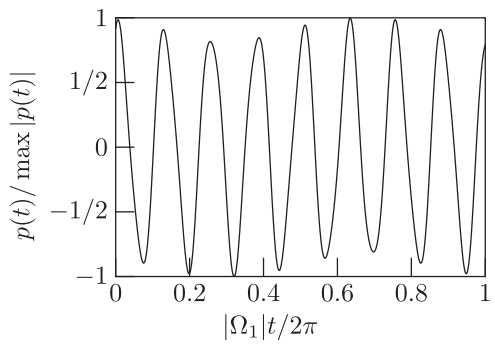

FIG. 4. Sample signal for CROR test case, time scaled on period of rotation of front rotor, pressure scaled on maximum absolute value.

C. Broadband volume source

As a final example we compute the broadband signal radiated from a random volume source, modeled as a collection of point sources,

$$p(\mathbf{x},t) = \sum_{i=1}^{N_s} \frac{a_i \cos(\Omega_i \tau)}{4\pi R_i}$$
$$R_i = |\mathbf{x} - \mathbf{x}_i|, \quad \mathbf{x}_i = \rho_i(\sin\theta_i \cos\phi_i,\ \sin\theta_i \sin\phi_i,\ \cos\theta_i),$$
$$\tau = t - R_i/c, \tag{22}$$

where a_i, ρ_i, θ_i, and ϕ_i are randomly assigned with $-1/2 < a_i < 1/2$, $\rho_i < 2^{-1/2}$, $0 \le \theta_i < \pi$, and $0 \le \phi_i < 2\pi$. Frequency Ω_i is randomly assigned with $\Omega_1 \le \Omega \le \Omega_2$. For these calculations, $\Omega_1 = 1000$ and $\Omega_2 = 2000$ giving a one octave bandwidth for the signal. Randomization of the source amplitudes introduces partial cancellation effects which complicate the source directivity and random distribution of the point sources forms a volume source within the sphere, which is again of unit radius.

Calculations were performed with $N_\theta = N_\psi = 32$ and a varying time step, with third-order time interpolation. A sample time record is shown in Fig. 6, demonstrating that the signal is indeed random and broadband. The error in the radiated signal is shown as a function of time step in Fig. 7, for varying numbers of point sources. It is clear that the error is independent of the number of sources and that reducing the time step rapidly reduces the error as in the previous test case, showing that the accuracy of the method is not limited by geometric discretization in this case.

D. Computation time

Combining the results from the test cases, we can present an assessment of the computational time required for field calculations. The computation time for one time point at one position on a ray is made up of one matrix multiplication per ray, plus a sequence of multiplications per point on

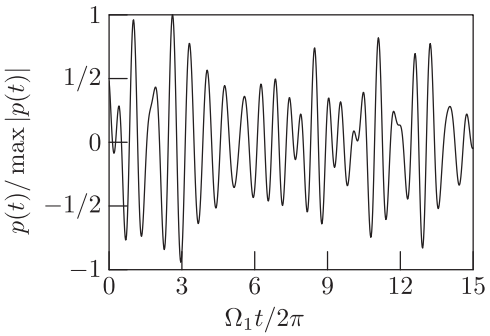

FIG. 6. Sample signal for broadband test case, time scaled on minimum source frequency, pressure scaled on maximum absolute value.

the ray. We present timing data for these computations as a function of grid resolution. There is also a pre-processing stage in generating the surface data on the spherical grid. The time required for this stage will vary depending on implementation and application, but for completeness, we present it here for the worst case, when it is computed using a direct field calculation at each node. In practice, we expect that the spherical surface data would be generated as part of another calculation, for example, by interpolating from data generated during a CFD computation. In this case, the pre-processing cost is negligible. For error assessment, a direct calculation at each node is a better way of testing our algorithm, and so we have used this approach in the previous examples and present timing data based on this method.

The performance of the method is summarized by presenting the time required for a full-field calculation. We assume that in order to resolve the radiated field, it must be computed on a set of spherical grids of the same resolution as for the Kirchhoff surface, i.e., that the same aliasing and interpolation considerations apply in the field as near the source. The computational effort for the fast method is then

$$T_f = t_p + N_p t_r + n_r N_p t_c, \tag{23}$$

where t_p is the pre-processing time required to compute the surface quantities on the Kirchhoff surface, t_r is the pre-processing time for one radial vector, t_c is the computation time for one point on a radial vector, and n_r is the number of spherical surfaces, or radii, where the field is required. The corresponding computation time using direct evaluation is

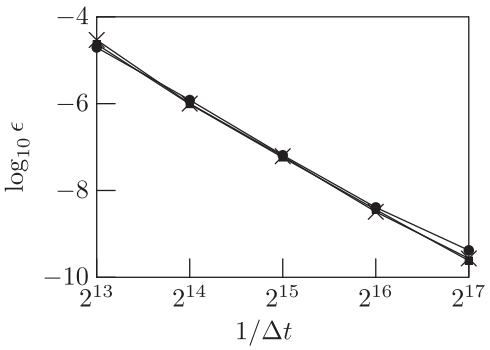

FIG. 7. Error versus time step for broadband test case with $N_\theta = 32$, $N_\psi = 32$, third-order time interpolation: circles $N_s = 1024$; squares $N_s = 4096$; crosses $N_s = 16384$.

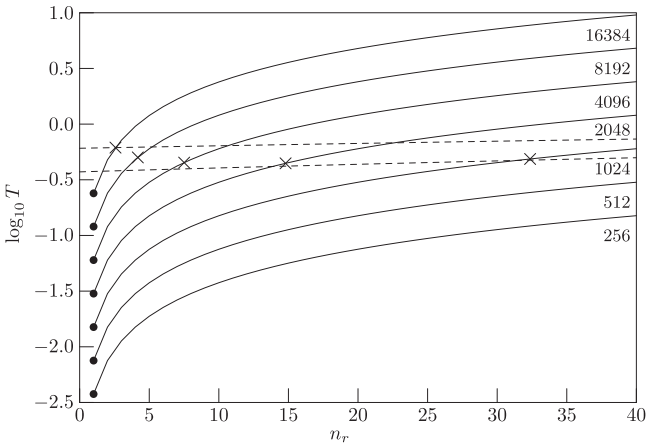

FIG. 8. Computation time for direct and fast methods with $N_\theta = 32$ ($N_p = 2048$) and $N_\psi = 32$: solid curves, T_d for $N_s = 256$, 512,…, 16 384; dashed lines, fast method for $N_s = 256$ (lower) and $N_s = 16\,384$ (upper); solid circles, pre-processing time for fast method; crosses, break-even point $T_f = T_d$.

$$T_d = n_r N_p t_d, \tag{24}$$

where t_d is the computation time for direct evaluation at one point. Computation times are scaled on the number of time points in the computed signal.

Figure 8 shows the computation time as a function of n_r and N_s. Other parameters were fixed at $N_\theta = 32$ ($N_p = 2048$), $N_\psi = 32$. Changing these values moves the curves for T_f up or down on the plot, but the general behavior is unaltered. The curves for T_f appear flat because of the very small value of t_c: the main computational burden appears in the pre-processing stage, t_p, but the marginal cost of computing at one radius is negligible. Because of the approach taken, t_p scales as $N_p N_s$, while t_r scales as $N_p N_\psi$ and t_c as N_ψ. In our implementation, t_p is up to three orders of magnitude greater than t_r which is in turn two orders of magnitude greater than t_c. The pre-processing time t_p is shown as a solid circle and is the same as t_d for $n_r = 1$, as it obviously should be. Also shown as crosses are the points where $T_d = T_f$ and the time for the fast method breaks even with direct evaluation. For small numbers of sources, the fast approach is not competitive with direct computation, as might be expected, but for large N_s, it quickly demonstrates its superiority. The break-even value of n_r roughly halves as N_s doubles and for $N_s = 16\,384$, if the field is required on spheres at more than two radii our algorithm is already faster than direct evaluation.

We also note that if the input data are not computed from an array of point sources, but interpolated from CFD data say, the pre-processing cost t_p is negligible.

IV. CONCLUSIONS

We have presented a method for the efficient evaluation of transient acoustic fields which uses standard methods and demonstrates good accuracy and computational effort on realistic test cases. The approach can also be used with interpolated CFD data at negligible computational cost, so that it offers a rigorous and systematic means of computing radiated fields from computed flow data, as well as from

collections of point sources. The break-even point where our method is faster than direct evaluation has been considered and, while dependent on problem size, demonstrates that when a full field calculation is to be performed, our algorithm is superior to direct evaluation even for modest problem sizes and very much faster as the number of sources increases.

[1]A. D. Pierce, *Acoustics: An Introduction to its Physical Principles and Applications* (Acoustical Society of America, New York, 1989), p. 182.
[2]H. L. Oestreicher, "Representation of the field of an acoustic source as a series of multipole fields," J. Acoust. Soc. Am. **29**(11), 1219–1222 (1957). See Ref. 14.
[3]Y. Mao and C. Xu, "Accelerated method for predicting acoustic far field and acoustic power of rotating source," AIAA J. **54**(2), 603–615 (2016).
[4]P. Croaker, N. Kessisoglou, R. Kinns, and S. Marburg, "Fast low-storage method for evaluating Lighthill's volume quadrupoles," AIAA J. **51**(4), 867–884 (2013).
[5]F. Margnat, "A fast procedure for the computation of acoustic fields given by retarded-potential integrals," in *16th AIAA/CEAS Aeroacoustics Conference*, 2010.
[6]F. Margnat and V. Fortuné, "An iterative algorithm for computing aeroacoustic integrals with application to the analysis of free shear flows," J. Acoust. Soc. Am. **128**(4), 1656–1667 (2010).
[7]M. Carley, "Fast evaluation of transient acoustic fields," J. Acoust. Soc. Am. **139**(2), 630–635 (2016).
[8]A. S. Lyrintzis, "Surface integral methods in computational aeroacoustics—From the (CFD) near-field to the (Acoustic) far-field," Int. J. Aeroacoust. **2**(2), 95–128 (2003).
[9]P. N. Swarztrauber, "On the spectral approximation of discrete scalar and vector functions on the sphere," SIAM J. Numer. Anal. **16**(6), 934–949 (1979).
[10]Z. Gimbutas and L. Greengard, "A fast and stable method for rotating spherical harmonic expansions," J. Comput. Phys. **228**, 5621–5627 (2009).
[11]D. Casalino, "An advanced time approach for acoustic analogy predictions," J. Sound Vib. **261**(4), 583–612 (2003).
[12]M. Kessler and S. Wagner, "Source-time dominant aeroacoustics," Comput. Fluids **33**, 791–800 (2004).
[13]T. Deconinck, A. Capron, C. Hirsch, and G. Ghorbaniasl, "Prediction of near- and far-field noise generated by contra-rotating open rotors," Int. J. Aeroacoust. **11**(2), 177–196 (2012).
[14]H. L. Oestreicher, "Erratum: Representation of the field of an acoustic source as a series of multipole fields [J. Acoust. Soc. Am. **29**, 1219 (1957)]," J. Acoust. Soc. Am. **30**(5), 481–481 (1958).